

A photometric study of V608 Cam: apparent period changes as a result of surface activity

F. Šebek^{a,b}, F. Walter ^{b,c}, M. Wolf^d

^aHigh School Botičská, Botičská 1, CZ-128 01 Praha 2, Czech Republic

^bCzech Astronomical Society, Variable Star and Exoplanet Section, Vídeňská 1056,
CZ-142 00 Praha 4, Czech Republic

^cStefanik Observatory Prague, Strahovská 205, CZ-118 00 Praha 1, Czech Republic

^dAstronomical Institute, Faculty of Mathematics and Physics, Charles University,
V Holešovičkách 2, CZ-180 00 Praha 8, Czech Republic

Abstract

The VRI light curves were measured for the low-mass eclipsing binary V608 Cam as a part of our long-term observational project for studying of eclipsing binaries with a short orbital period. The TESS light curve solution in PHOEBE results to the detached configuration, where the temperature of primary component was fixed to $T_1 = 5300$ K according to GAIA results, which gives us $T_2 = 4110 \pm 50$ K for the secondary. The spectral type of the primary component was derived to be K0 and the photometric mass ratio was estimated $q = 0.92 \pm 0.07$. Characteristics and temporal variation of the cold region on the surface of the secondary component were estimated and are attributed to apparent period changes of this eclipsing binary with a cycle of about 2.4 yr.

Keywords: binaries: eclipsing; binaries: close; binaries: low-mass; stars: activity; stars: fundamental parameters; stars: individual: V608 Cam;

1. Introduction

Low-mass and late-type stars with masses below $1 M_\odot$ (spectral types K and M) are the most common and most frequent stars in our Galaxy. Long-term photometric monitoring of low-mass eclipsing binaries is a very useful tool for studying star-spot parameters (their structure, coordinates, sizes and temperatures), their evolution and statistical properties. Nevertheless, current observations of low-mass stars show a long-lasting discrepancy between estimated and modeled parameters, where the models give 5–10 % smaller radii than observations (Chabrier & Baraffe 2000; Morales et al. 2010; Mann et al. 2015). The low-mass stars are also affected by chromospheric activity caused by a strong magnetic field, dark or bright spots. This variable activity has been frequently observed as flares, and plays important role for precise determination of fundamental physical parameters, esp. their radii and temperatures. Their rotation periods are synchronized with the orbital period due to the tidal forces.

Moreover, many low-mass eclipsing binaries display periodic eclipse time variations caused by a third circumbinary component orbiting the eclipsing pair

Email address: filip.sebek.fs@gmail.com (F. Šebek)

(so-called Light-Time Effect, LITE, Irwin 1952) or magnetically-induced modulations caused by an active star in the system (Applegate 1992). This makes them very promising targets to search for circumbinary brown dwarfs or giant planets by analyzing the LITE. To date, several substellar companions to LMBs have been discovered using this simple but efficient method (Lee et al. 2009; Hinse et al. 2012; Pribulla et al. 2012).

Additional timing variations with small amplitudes might be produced by the asymmetries of the eclipse light curves through stellar activity, such as star spots or small flares. The effect of star spots on the $O-C$ diagrams was studied by Kalimeris et al. (2002). They found that star spots modulate the $O-C$ values and can introduce high-frequency and low-amplitude disturbances of less than 0.01 d. These variations are caused by the change in the surface density and center of light over the visible hemisphere. Barros et al. (2013) showed that observed transit time variations in the hot-Jupiter WASP-10b system are also due to spot occultation features. Moreover, Korda et al. (2017) tested the spot variability on the light curve of low-mass binaries and found a difference in mid-eclipse times of about 95 s. Recently, Zaire et al. (2022) announced, that the well-known eclipsing binary system V471 Tau has the magnetically active K2 dwarf component, which might be responsible for driving the eclipse timing variations with predicted ~ 35 yr activity cycle.

The low-mass eclipsing binary V608 Cam (also NSVS 109935, BD+82 160, ASASSN-V J062601.90+822126.3, 1RXS J062558.2+822124, TYC 4537-0765, Sp. K0, $V_{\max} = 10.6$ mag) is a rather bright but neglected northern object with a short orbital period of about 10 h. In the SIMBAD¹ database V608 Cam is also mentioned as a nearby and high proper-motion star. Its variability was discovered by Hoffmann et al. (2008) using the publicly available Northern Sky Variability Survey (NSVS, Wozniak et al. 2004) and classified as a probable low-mass binary with the period of 0.448 d.

V608 Cam is also listed as an object 1RXS J062558.2+822124 in the ROSAT All-Sky Bright Source Catalogue (Voges et al. 1999) as a faint X-ray source. For V608 Cam the angular diameter of the system $\rho = 7.84 \cdot 10^{-2}$ mas was also measured by the GAIA satellite and this value is included in the *Mid-infrared stellar Diameters and Fluxes compilation Catalogue* (MDFC ver. 10, Cruzalebes et al. 2019). Recently, V608 Cam was included in a study of nearby young stellar association in Cepheus and classified as a spectroscopic binary of SB1 type (Klutsch et al. 2020). The following linear ephemeris was proposed in the VSX-index² for the current use:

$$\text{Pri.Min.} = \text{HJD } 24\,57762.8815 + 0.448072 \cdot E. \quad (1)$$

The GAIA DR2 astrometric and photometric data on V608 Cam are summarized in Table 1 (Gaia Collaboration et al. 2018). The distance to the system was derived to be $d = 115.6 \pm 0.2$ pc (Bailer-Jones et al. 2021).

In this paper we report on a light curve model and surface activity on one component of this low-mass and late-type eclipsing binary. To our knowledge, no precise photometric analysis nor period study of V608 Cam has been published so far. The presented paper is structured as follows. In Section 2, we describe

¹<http://simbad.u-strasbg.fr/simbad/>

²<https://www.aavso.org/vsx/>

Table 1: GAIA DR2 astrometric and photometric data on V608 Cam.

Parameter	Value
α_{2000} [h m s]	06 26 01.76
δ_{2000} [d m s]	+82 21 27.59
pm α [mas/yr]	0.510 ± 0.020
pm δ [mas/yr]	-50.320 ± 0.016
parallax [mas]	8.631 ± 0.013
B [mag]	11.53 ± 0.07
V [mag]	10.658 ± 0.013
G [mag]	10.465 ± 0.007
BP [mag]	10.836 ± 0.013
RP [mag]	9.833 ± 0.013
J [mag]	9.277 ± 0.020
H [mag]	8.874 ± 0.015
K [mag]	8.771 ± 0.020

our photometric observations and data analyses. The improved ephemeris is also derived. The new mid-eclipse times and $O-C$ diagram is presented in Section 3. In Section 4, we analyse V608 Cam light curves and derive photometric parameters of the system. The discussion of the results is given in Section 5 and our conclusions are presented in Section 6.

2. Observations

Since 2020 the time-resolved CCD photometry of V608 Cam, mostly during eclipses, has been regularly obtained at two observatories.

- The initial CCD photometry was performed at Štefánik Observatory in Prague, Czech Republic, during Apr – Sep 2020. The 0.37-m Maksutov-Cassegrain telescope with the CMOS camera ZWO ASI 1600 MM Pro and VRI photometric filters were used. The mean exposure time was 45 sec.
- The next observations in our campaign were obtained at Valašské Meziříčí observatory, Czech Republic, during Sep – Oct 2021. The 0.15-m Newtonian telescope with remote control, the CCD camera MI G2-1600 and VRI filters were used. Individual exposure times lasted up to 60 sec. The folded VRI light curves are shown on Fig. 2.
- Finally, additional CCD photometry was performed at Valašské Meziříčí observatory in March 2022. The 0.15-m Newtonian telescope with remote control, the CCD camera MI G2-1600 and SLOAN g, r, i filters were used. Individual exposure times lasted up to 70 sec.

Smaller telescopes and modern CCD technique were sufficient for good S/N photometry of such a bright object. Our CCD observations were reduced in a standard way. The images were bias-corrected and flat-fielded before aperture

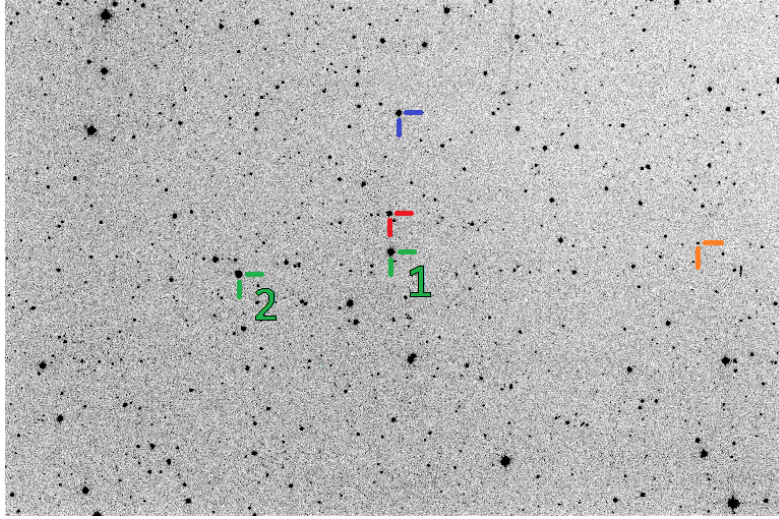


Figure 1: The finding chart of V608 Cam, the dimensions are approx. $1^\circ \times 42'$, north is right. The position of variable (red), comparison 1 and 2 (green) and check (blue) stars are denoted. The nearby variable NSVS 108681 is marked orange.

Table 2: Precise coordinates of selected stars in the field of V608 Cam, see Fig. 1.

Object	α_{2000} [h:m:s]	δ_{2000} [d:m:s]	V [mag]	Other name
V608 Cam	06 26 01.76	+82 21 27.59	10.6	BD+82 160
comparison1	06 27 34.53	+82 21 51.04	9.55	BD+82 161
comparison2	06 29 01.16	+82 09 53.80	10.23	BD+82 163
check	06 21 57.23	+82 21 17.60	10.80	GSC 04537-00881

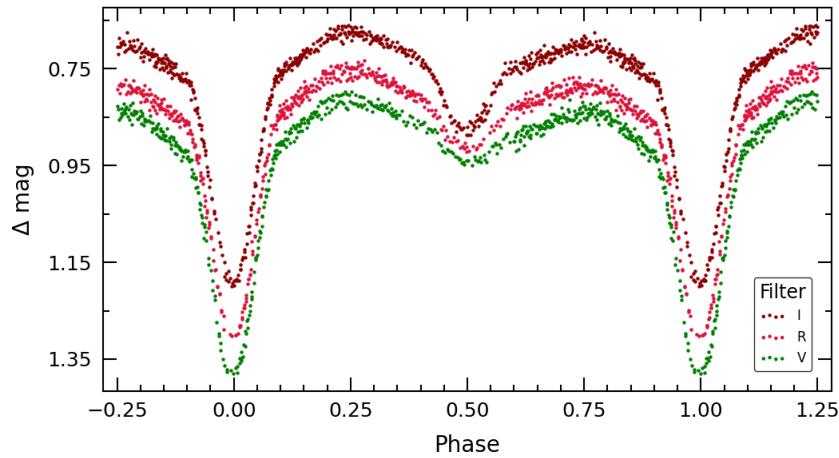


Figure 2: The VRI differential light curves of V608 Cam obtained during Sep - Oct 2021 at Valašské Meziříčí.

photometry was carried out. The C-MUNIPACK³, a synthetic aperture photometry software, was routinely used. Time-series were constructed by computing the magnitude difference between the variable and a nearby comparison and check stars, see Fig. 1 and Table 2. The heliocentric correction was applied. The computer at the Štefánik Observatory telescope is synchronized using the local Meinberg NTP⁴ service using five different NTP time-servers as time reference. Resulting local time is smoothed average of differences to all reference servers. Computer at Valašské Meziříčí Observatory is periodically synchronized using a time-server provided by Microsoft. The uncertainties of photometric measurements at two smaller telescopes were always about 0.01 – 0.02 mag.

As a northern object with high declination (Dec. $\simeq +82^\circ$), V608 Cam was also measured frequently by the *Transiting Exoplanet Survey Satellite* (TESS) in 2-min cadence during several periods (Sectors 19 and 20 in 2019, Sectors 40 and 47 in 2021, and Sector 52 in Dec 2022). These high-quality light curves were used for precise mid-eclipse time determination as well as for modeling of the system. New times of primary and secondary minima and their uncertainties were generally determined by fitting the light curve by Gaussians or polynomials of the third or fourth order. The least-squares method was used. They are listed in Table 3, where epochs were computed according to the following improved linear ephemeris:

$$\text{Pri.Min.} = \text{HJD } 24\,51474.6316(13) + 0.44807272(8) \cdot E. \quad (2)$$

Minima obtained at Štefánik Observatory and Valašské Meziříčí were calculated as the mean value of *VRI* or *gri* measurements.

³Package of software utilities for reducing astronomy CCD images, current version 2.1.32, available at <http://c-munipack.sourceforge.net/>

⁴https://www.meinbergglobal.com/english/sw/ntp.htm#ntp_stable

Table 3: New TESS precise times of primary and secondary eclipses of V608 Cam.

BJD – 24 00000	Epoch	BJD – 24 00000	Epoch
<i>Sector 19</i>		<i>Sector 40</i>	
58816.30442	16385.0	59390.73118	17667.0
58816.52814	16385.5	59390.95830	17667.5
58817.64862	16388.0	59395.21180	17677.0
58818.99290	16391.0	59395.43938	17677.5
58826.83337	16408.5	59395.65992	17678.0
58830.86568	16417.5	59400.58914	17689.0
58831.09045	16418.0	59400.81648	17689.5
58831.31380	16418.5	59409.99947	17710.0
58831.53838	16419.0	59410.22612	17710.5
58840.72242	16439.5	59418.06483	17728.0
58840.94787	16440.0	59418.29167	17728.5
<i>Sector 20</i>		59418.51314	17729.0
58842.74013	16444.0	59418.73930	17729.5
58842.96261	16444.5	<i>Sector 47</i>	
58845.87647	16451.0	59580.04531	18089.5
58846.09935	16451.5	59580.26636	18090.0
58849.68331	16459.5	59585.64355	18102.0
58849.90907	16460.0	59588.55799	18108.5
58850.35711	16461.0	59590.12448	18112.0
58850.57951	16461.5	59592.14277	18116.5
58856.85193	16475.5	59592.81277	18118.0
58857.07832	16476.0	59595.72704	18124.5
58860.21499	16483.0	59595.94930	18125.0
58860.43710	16483.5	59598.63754	18131.0
58868.28071	16501.0	59602.89581	18140.5
58868.50233	16501.5	59603.11833	18141.0
58868.72892	16502.0	59606.48101	18148.5
–	–	59606.70294	18149.0

Table 4: New and collected times of primary and secondary eclipses of V608 Cam.

BJD – 24 00000	Epoch	Error [day]	Observer/ Source
51474.62908	0.0	–	Hoffmann et al. (2008)
55478.61116	8936.0	0.0002	Dubovský
56356.38667	10895.0	0.0004	Hübscher (2013)
56371.62247	10929.0	0.0018	Hübscher (2013)
57080.47168	12511.0	0.0008	Hübscher (2016)
57296.43789	12993.0	0.0007	Hübscher (2017)
57815.30651	14151.0	0.0011	Pagel (2018)
58083.25282	14749.0	0.0001	Screech
58115.29208	14820.5	0.0003	Screech
58138.36421	14872.0	0.0003	Screech
58174.43909	14952.5	0.0005	Screech
58174.65936	14953.0	0.0001	Screech
58245.45848	15111.0	0.0001	Screech
58418.41320	15497.0	0.0001	Screech
58506.45857	15693.5	0.0004	Dienstbier
58764.54982	16269.5	0.0004	Pagel (2021)
58887.32392	16543.5	0.0017	Pagel (2021)
58887.54772	16544.0	0.0013	Pagel (2021)
58957.44818	16700.0	0.0002	1
58961.48087	16709.0	0.0001	1
59107.55265	17035.0	0.0001	Screech
59110.46119	17041.5	0.0002	1
59113.59834	17048.5	0.0002	1
59275.35892	17409.5	0.0094	Pagel (2022)
59275.58022	17410.0	0.0022	Pagel (2022)
59465.55996	17834.0	0.0002	2
59466.45638	17836.0	0.0001	2
59663.38181	18275.5	0.0005	2
59663.60753	18276.0	0.0001	2
59664.27982	18277.5	0.0003	2
59664.50386	18278.0	0.0001	2
59666.51932	18282.5	0.0003	2
59681.30668	18315.5	0.0008	Kamenec
59684.44221	18322.5	0.0008	Kamenec
59727.45761	18418.5	0.0001	1

Observatory: 1 - Štefánik Observatory, 2 - Valašské Meziříčí

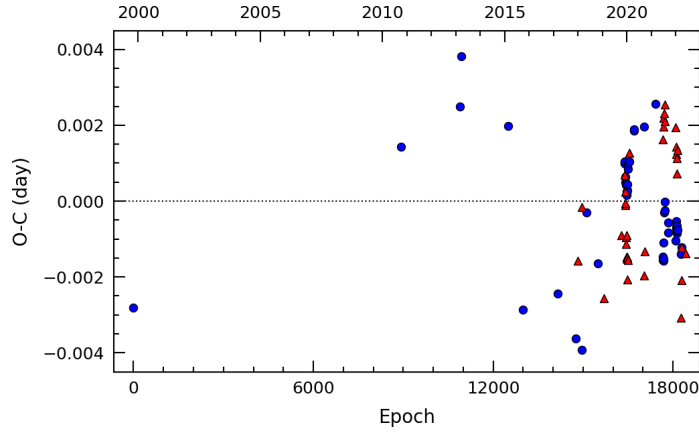


Figure 3: The current $O-C$ diagram for the times of minimum of V608 Cam since discovery. The individual primary and secondary CCD minima are denoted by blue circles and red triangles, respectively.

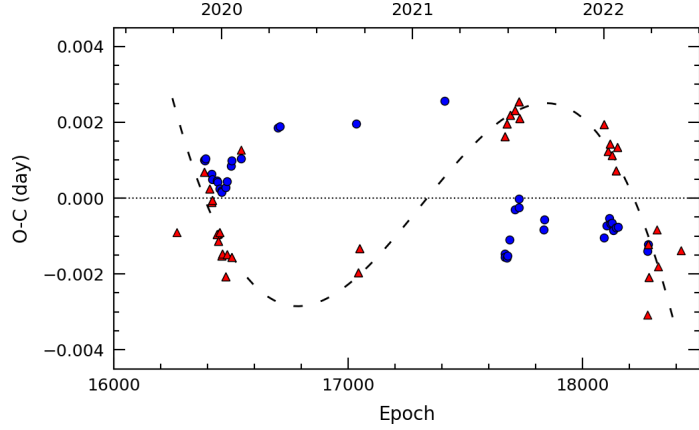


Figure 4: The $O-C$ diagram in detail for the times of minimum of V608 Cam since the first TESS data. The change of $O-C$ values for primary and secondary eclipses very probably caused by stellar surface activity is clearly visible. The quasi-sinusoidal fit for secondary minima with a semi-amplitude of about 0.003 day is plotted as the dashed black curve.

3. O-C diagram

The period changes of V608 Cam had not been studied since its discovery. Only a few eclipse timings have been reported in the literature. Using the TESS data we derived 54 new mid-eclipse times to complete our current $O-C$ diagram. These times divided into four groups according to different TESS sectors are included in Table 3. Their uncertainty was fixed to 0.00001 day although the least squares fit of the light curve during the eclipse gives us formally smaller values. On the other hand, the scatter of TESS minima is surprisingly larger than the given error. Besides those minima given in Table 3, we also used previous times of minimum published by Hübscher (2013, 2016, 2017) and Pagel (2018,

2021, 2022), and those collected in the $O-C$ Gateway⁵.

Additional minima were obtained from photometric data available at the BAA Photometry Database⁶. These observations were carried out by James T. Screech using the 0.07-m refractor and CMOS Camera ASI 1600MM-C. Five additional minima have been obtained by Pavol Dubovský using 400 mm photo-lens and CCD camera SXVF-H9, by Vojtěch Dienstbier using the 0.15-m Newtonian telescope and CCD camera MI G2-1600, by Matúš Kamenec using the SkyWatcher 102/500 telescope and the Canon EOS 500D camera and finally again at Štefánik Observatory using 0.4-m Schmidt-Cassegrain telescope and the SBIG ST10-XM CCD camera.

Because the TESS data are provided in the Barycentric Julian Date Dynamical Time (BJD_{TDB}), all our times in Table 3 were first transformed to this time scale using the often used Time Utilities of Ohio State University⁷ (Eastman et al. 2010). A total of 88 precise CCD times including 37 secondary eclipses were used for the period determination. The computed linear light elements and their internal errors of the least-squares fit are given in Eq. 2, the historical $O-C$ diagram is shown in Fig. 3, the $O-C$ diagram for the current mid-eclipse times in detail is plotted in Fig. 4.

As one can see, the current accurate mid-eclipse times show a relatively large scatter. There are no clear indications for regular cyclical changes of the orbital period caused f.e. by a third component and observed as LITE. Moreover, the shallower secondary eclipses show some cyclic trend of their $O-C$ values because they are probably more sensitive to some surface inhomogenities of the secondary component, see Fig. 4. This effect was further studied by a light-curve solution. The observable difference in mid-eclipse times of spotted components was also outlined recently by Korda et al. (2017).

4. Light curve solution

No photometric or spectroscopic solution has been reported for V608 Cam so far. Comparison of our light curves obtained in different epochs with the TESS data clearly show rapid changes of their shape, especially out of eclipse around phases 0.25 and 0.75, see Fig. 5. All light curves of V608 Cam obtained during 2020–2021 at our disposal were analyzed using the well-known PHOEBE⁸ code (Prša & Zwitter 2005, Prša et al. 2016), which is based on the Wilson-Devinney algorithm (Wilson & Devinney 1971) and is widely used for modeling the photometric light curves of eclipsing binaries as a standard tool. Because V608 Cam belongs to late-type binaries, we adopted the bolometric albedos and gravity darkening coefficients as $A_1 = A_2 = 0.5$ and $g_1 = g_2 = 0.32$, which corresponds to the convective envelopes. Synchronous rotation for both components of the system ($F_1 = F_2 = 1$) and a circular orbit ($e = 0$) were assumed. We used the logarithmic limb-darkening law with the coefficients adopted from van Hamme (1993) tables. The temperature of the primary component was fixed to the value of 5 300 K given in the GAIA DR2 Archive. This value is in good agreement

⁵<http://var2.astro.cz/ocgate/>

⁶<https://britastro.org/photdb/data.php>

⁷<http://astrutils.astronomy.ohio-state.edu/time/>

⁸<http://phoebe-project.org/>

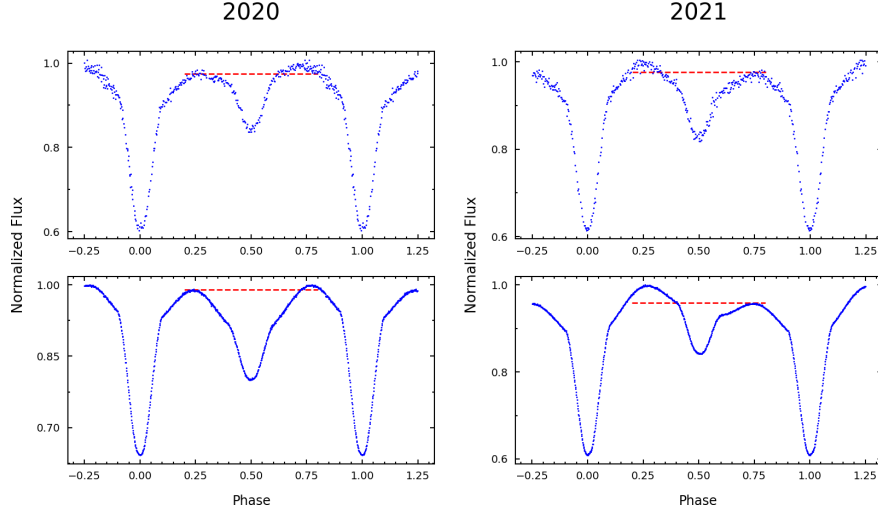


Figure 5: Comparison of light curves obtained in 2020 and 2021. The first row corresponds to the light curves obtained at Štefánik Observatory and at Valašské Meziříčí, the second row corresponds to the TESS light curves, sectors 20 and 40. Changes of brightness in both quadratures are denoted by red dashed lines.

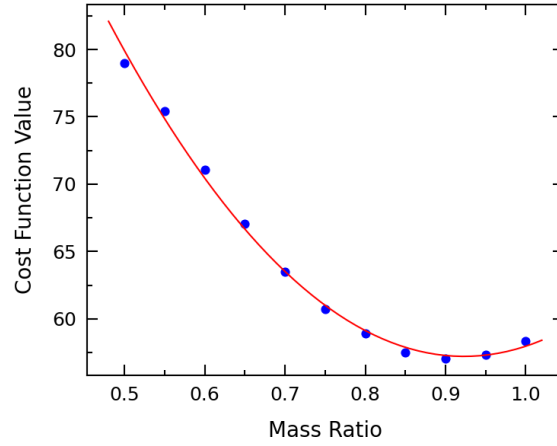


Figure 6: The result of the q -search for the TESS light curve.

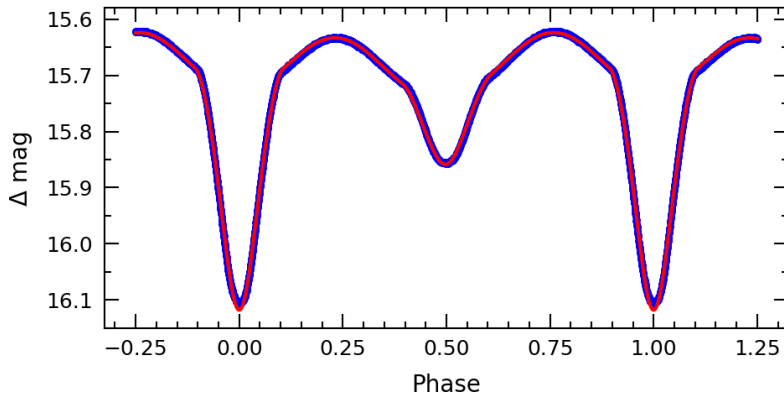


Figure 7: The PHOEBE final solution for the TESS light curve, Sector 20. The TESS data are denoted blue, the resulting model in red.

with the color index $B - V = 0.872$ mag and $J - H = 0.403$ mag given in the SIMBAD database. Also the table of Pecaut & Mamajek (2013)⁹ gives for this temperature the similar color indexes $B - V = 0.816$ mag, $J - H = 0.387$ mag and the same spectral type K0.

In the absence of the spectroscopic mass ratio, the q -search process was performed to find a corresponding photometric mass ratio. Assuming a given mass ratio q from the interval of (0.5,1) in step of 0.05, we let converge the other parameters. At first we fitted those parameters that had a substantial effect on the shape of light curves. The adjustable parameters were thus the inclination i , the effective temperature of the secondary component T_2 , luminosity and dimensionless potentials of both components Ω_1, Ω_2 . Next, the characteristics of a cold spot/region on the secondary component (colatitude, longitude, spot radius and temperature factor) were included. This method of the direct mass ratio and spot parameters estimation from the eclipsing binary light curve was recently evaluated by Terrell (2022). Because the effective temperature and the radius of a spot are strongly correlated, we assumed that the ratio of spot/star temperatures is close to 0.9 in our analyzes. No third light L_3 was included to the light curve solution. The fine and coarse grid raster for both components were set to 30. The minimum value of the cost function was achieved at $q = 0.92 \pm 0.07$, see also Fig. 6.

As a first attempt we selected roughly 1000 points of the precise TESS light curve obtained in the Sector 20, to obtain basic photometric parameters of the system, see Fig. 7 and Table 5. The wavelength coverage of TESS is about 6000 – 10000 Å, covering most of the R and I filters. As one can see, the agreement between the theoretical and observed light curve is very good. Both additional light curves obtained in Štefánik Observatory and Valašské Meziříčí were then solved independently to estimate primarily the characteristics of the dark region. All of available light curves in different filters obtained in one season were fitted simultaneously. Numerous PHOEBE 1 runs in a detached mode using the different setup of initial parameters were evaluated. The results

⁹http://www.pas.rochester.edu/~emamajek/EEM_dwarf_UBVIJHK_colors_Teff.txt

Table 5: The photometric elements of V608 Cam, the PHOEBE solution.

Parameter	Primary	Secondary
i [deg]	73.8	
q	0.92 (fixed)	
$T_{1,2}$ [K]	5300 (fixed)	4110
$\Omega_{1,2}$	3.879	4.256
$X_{1,2}$	0.703	0.735
$r(pole)$	0.333	0.284
$r(side)$	0.346	0.291
$r(point)$	0.387	0.309
$r(back)$	0.365	0.302

Table 6: Absolute parameters of V608 Cam, based on TESS photometry and color indexes.

Parameter	Primary	Secondary
Mass [M_{\odot}]	0.88	0.81(6)
Radius [R_{\odot}]	1.02(4)	0.86(7)
Luminosity [L_{\odot}]	0.74(6)	0.19(3)
M_{bol} [mag]	5.06(9)	6.55(19)
a [R_{\odot}]	2.94(3)	

as well as the cost function value were recorded.

The need to include spots to the final solution was evident in view of the modulation of out-of-eclipse light curves. We also made some preliminary tests placing spot on both components at latitudes of 45 deg, which is the region most affected by spots in low-mass stars (Granzer et al. 2000).

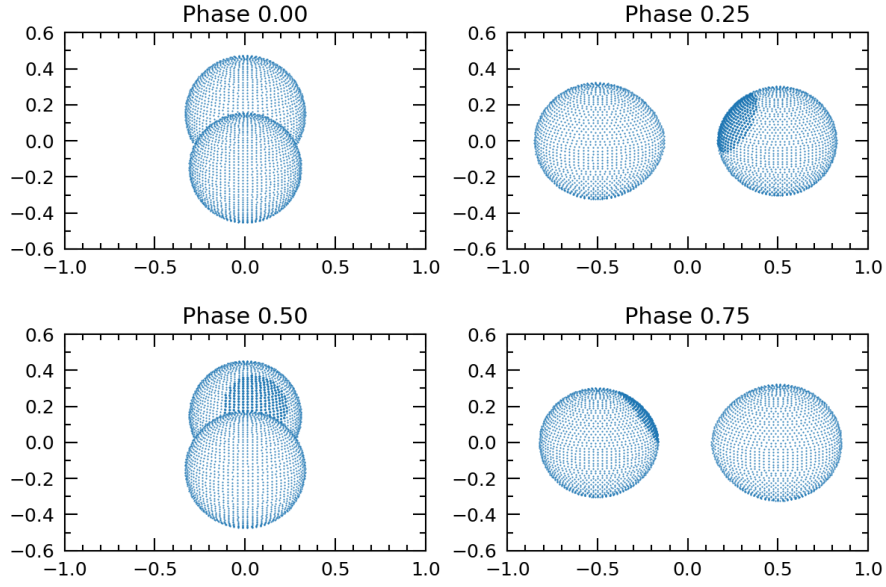
Finally, for a given temperature, the mass of the primary component $M_1 = 0.88 M_{\odot}$ was adopted. Then the semi-major axis $a = 2.935 R_{\odot}$ was fixed to an appropriate value for the primary mass to be equal to a typical mass of a particular spectral type (Pecaut & Mamajek 2013). With this approach, we were able to estimate the preliminary masses, in addition to the radii and luminosities of both components in absolute units (see Table 6).

The final light curve solution is given in Table 5, where also bolometric limb-darkening coefficients and relative radii of both components are given. The resulting parameters of the cold region on the secondary are given in Table 7. The geometrical representation of V608 Cam in two epochs is displayed in Fig. 8.

5. Discussion

In Table 6 we collected absolute parameters of V608 Cam directly derived from the light curves or estimated from the color indexes. The mass of primary component was taken from the table of Pecaut & Mamajek (2013) according to its GAIA temperature. The other quantities in Table 6 were derived directly from the light curve solution in PHOEBE.

Jan 2020 - TESS (sector 20)



Oct 2021 - Valašské Meziříčí

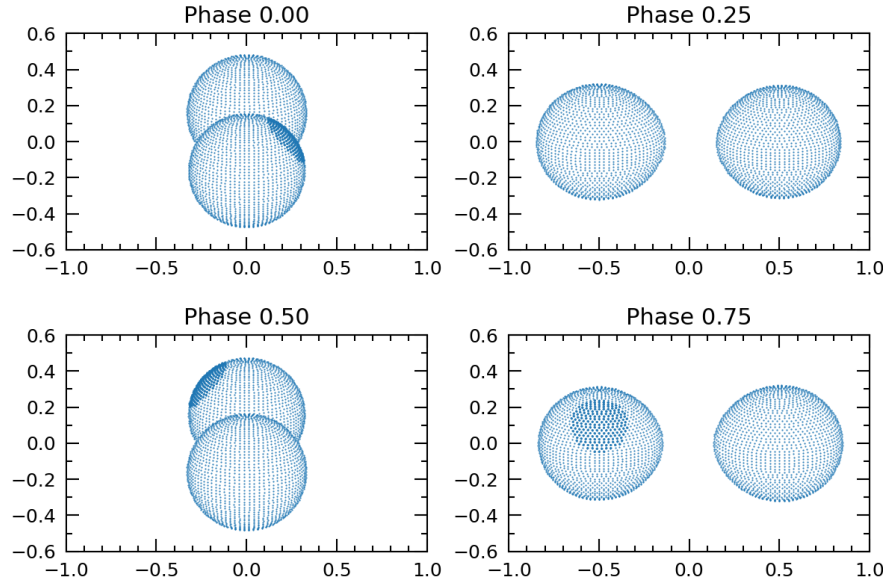


Figure 8: The geometry of V608 Cam in two epochs. The detached configuration with the large cold region on the secondary component is visible in the TESS data as well as in our photometry obtained at Valašské Meziříčí.

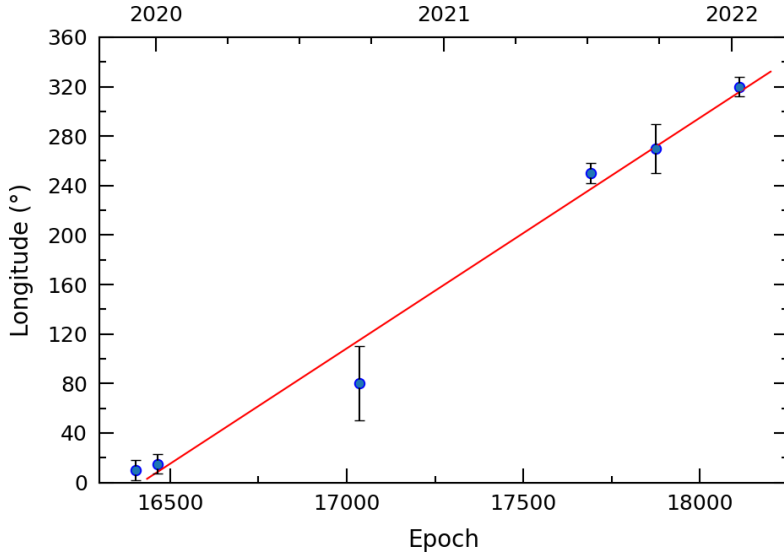


Figure 9: The gradual increase in longitude of the cold structure on the surface of the secondary component during several observational epochs. The calculated slope of the red line (0.185 deg/epoch) corresponds to a rate of 12.5 deg/month. Mean errors in longitude are indicated.

Moreover, for the GAIA parallax given in Table 1 and the angular diameter of the system $\rho = 7.84 \cdot 10^{-2}$ mas (Cruzalebes et al. 2019), one can obtain for the distance of V608 Cam a linear dimension $D = 1.96 R_{\odot}$, which is in good accordance with the derived values of radii $R_1 + R_2 = 1.88 R_{\odot}$ (see Table 6). No flare-like event was recorded during our photometric monitoring as well as on the precise TESS light curves.

On the other hand, the seasonal light curve of V608 Cam shows slowly evolving starspot structures that also strongly affect the estimation of precise $O-C$ timings. The apparent period changes are better visible on the run of secondary eclipses and are probably caused by a moving cold structure on the surface of the secondary component, where a different part of this region is partially eclipsed. Fig. 9 shows a slow increase in the spot longitude during several epochs of TESS and our observations collected also in Table 7. Although the resulting colatitude and the radius of the dark structure remain practically the same, the value of its longitude changes at a mean rate about +12.5 deg/month. This value is in good agreement with the current $O-C$ diagram (Fig. 4), where secondary minima show a quasi-periodic behavior with a period about 2.4 years.

The similar result was obtained recently for the binary V1130 Cyg, where the active component has one spotted area migrating longitudinally on the stellar surface with a period of about 122 days (Yoldas & Dal, 2021). Star-spot activity was also studied in case of KIC 11560447 by Ozavci et al. (2018), where the rotation of active regions up to about 2.4 deg per day was found. The spot activity in Algol binary KIC 06852488 was recently presented by Shi et al. (2021). Using the Kepler and TESS light curves they found an evolving hot spot on the primary and a cold spot on the secondary component. Certain correlation between the O’Connell effect and the $O-C$ curve similar to our result was presented.

Table 7: Parameters of the cold surface structure on the secondary component of V608 Cam obtained using different data sets.

Data set	Epoch	Longitude [deg]	Colatitude [deg]	Radius [deg]	PHOEBE cost function
TESS 19	Dec 2019	10	70	35	108
TESS 20	Jan 2020	15	60	35	43
Štef. Obs.	Sep 2020	80	70	30	381
TESS 40	Jul 2021	250	70	35	118
Val.Mez.Obs.	Oct 2021	270	50	30	302
TESS 47	Jan 2022	320	70	35	52

One has to take into consideration that such small apparent variation in orbital period on a short time-scale, frequently attributed to the light-time effect caused by an unseen third body, could be simply a result of the dark-spot evolution or its movement on the surface of binary components.

6. Conclusions

A study of late-type and low-mass binaries provides us with important information about the most common stars in our Galaxy. The interesting system V608 Cam with a large cold region on the surface of the secondary component was studied. The new multi-color photometric observations of V608 Cam as well as TESS data were used to investigate its light curve and determine the photometric parameters of its components.

The system V608 Cam contains the more massive and warmer primary component with $M_1 = 0.88 M_\odot$. The mass of the secondary was determined $M_2 = 0.81 \pm 0.06 M_\odot$ and its effective temperature $T_2 = 4110 \pm 50$ K. The system inclination is $i = 73.8^\circ$. We can conclude that V608 Cam is a nearby low-mass, active and detached eclipsing binary.

Their apparent period changes are probably connected with magnetic activity and changes of position of the cold structure on the secondary component. The current $O-C$ diagram based primarily on TESS data shows quasi-periodic changes caused by surface activities and a systematic shift of secondary eclipses. Formally one could declare such behavior as a "false eccentricity" of the otherwise circular orbit. This phenomenon must also be included to possible explanations of period changes in many late-type binary systems explained so far by a magnetic field (so-called Applegate mechanism, Applegate 1992) or by the light-time effect (LITE) caused by a third component orbiting the eclipsing pair (Irwin 1952). Concerning the surface activity, the identification of V608 Cam as a faint X-ray source (Voges et al. 1999) also supports our findings.

New high-accuracy timings of this eclipsing binary are necessary to investigate the parameters derived in this paper. It is also highly desirable to obtain new, high-dispersion and high-S/N spectroscopic observations and to apply modern disentangling methods to obtain the radial-velocity curves and to derive accurate masses for this interesting late-type system.

7. Acknowledgments

The authors would like to thank Ladislav Šmelcer, Valašské Meziříčí observatory, and Zbyněk Henzl, Variable Star and Exoplanet Section, the Czech Astronomical Society, for their kind assistance with remote observation, and to Stanislav Boula and other employees of Štefánik Observatory for their support. The research of M.W. was supported by the project Progress Q47 PHYSICS of Charles University in Prague. This paper includes data collected by the TESS mission. Funding for the TESS mission is provided by the NASA’s Science Mission Directorate. This work has made use of data from the European Space Agency (ESA) mission GAIA¹⁰, processed by the GAIA Data Processing and Analysis Consortium (DPAC)¹¹. Funding for the DPAC has been provided by national institutions, in particular the institutions participating in the Gaia Multilateral Agreement. The following internet-based resources were used in research for this paper: the SIMBAD and VIZIER database operated at CDS, Strasbourg, France, the NASA’s Astrophysics Data System Bibliographic Services, the International Variable Star Index (VSX) database, operated at AAVSO, Cambridge, Massachusetts, USA, the British Astronomical Association, Photometry Database, and the Czech Astronomical Society B.R.N.O. photometry database of eclipsing binary stars minima and associated O-C Gateway database of minima timings. This research is part of an ongoing collaboration between professional astronomers, the Czech Astronomical Society, Variable Star and Exoplanet Section and the Planetum Prague, Štefánik Observatory.

8. Data Availability

The TESS and GAIA data underlying this paper is publicly available, the other photometric data are available on reasonable request to the authors.

References

- Applegate, J.H. 1992, *ApJ*, 385, 621
- Bailer-Jones, C.A.L., Rybizki, J., Fouesneau, M. et al. 2021, *AJ*, 161, 147
- Barros, S.C.C., Boué, G., Gibson, N.P., et al. 2013, *MNRAS*, 430, 3032
- Chabrier, G. & Baraffe, I. 2000, *ARA&A*, 38, 337
- Cruzalebes, P., Petrov, R.G., Robbe-Dubois, S., et al. 2019, *MNRAS*, 419, 3158
- Eastman, J., Siverd, R., Gaudi, B.S. 2010, *PASP*, 122, 935
- GAIA Collaboration, Brown, A.G.A., Vallenari, A., et al. 2018, *A&A*, 616, A1
- Granger, Th. et al. 2000, *A&A* 355, 1087
- Hinse, T.C., Lee, J.W., Gozdziewski, K., et al. 2012, *MNRAS*, 420, 3609
- Hoffman, D.I., Harrison, T.E., Coughlin, J.L., et al. 2008, *AJ*, 136, 1067
- Hübscher, J. 2013, *IBVS* No. 6084

¹⁰<https://www.cosmos.esa.int/gaia>

¹¹<https://www.cosmos.esa.int/web/gaia/dpac/consortium>

Hübscher, J. 2016, IBVS No. 6157

Hübscher, J. 2017, IBVS No. 6196

Irwin, J.B. 1952, ApJ, 116, 211

Kalimeris, A., Rovithis-Livaniou, H., Rovithis, P. 2002, A&A, 387, 969

Klutsch, A., Frasca, A., Guillout, P., et al. 2020, A&A, 637, A43

Korda, D., Zasche, P., Wolf, M. et al. 2017, AJ, 154, 30

Lee, J. W., Kim, S.L., Kim, C.H., et al. 2009, AJ, 137, 3181

Mann, A.W., Feiden, G.A., Gaidos, E., et al. 2015, ApJ, 804, 64

Morales, J.C., Gallardo, J., Ribas, I., et al. 2010, ApJ, 718, 502

Ozavci, I., Senavci, H.V., Isik, E. et al. 2018, MNRAS, 474, 5534

Pagel, L. 2018, IBVS No. 6244

Pagel, L. 2021, BAV Mitteilungen No. 252

Pagel, L. 2022, BAV Mitteilungen No. 254

Pecaut, M.J. & Mamajek, E.E. 2013, ApJS, 208, 9

Pribulla, T., Vanko, M., Ammler-von Eiff, M., et al. 2012, Astron. Nachr., 333, 754

Prša, A. & Zwitter, T. 2005, ApJ, 628, 426

Prša, A., Conroy, K.E., Horvat, M., et al. 2016, ApJS, 227, 29

Shi, X.-D., Qian, S.-B., Li, L.-J., et al. 2021, AJ, 161, 46

Terrell, D. 2022, Galaxies, 10, 8

Voges, W., Aschenbach, B., Boller, Th., et al. 1999, A&A 349, 389

van Hamme, W. 1993, Astron. J., 106, 2096

Wilson, R.E. & Devinney, E.J. 1971, ApJ, 166, 605

Wozniak, P.R., Vestrand, W.T., Akerlof, C.W., et al. 2004, AJ, 127, 2436

Yoldas, E. & Dal, H.A. 2021, Rev. Mex. Astron. Astrophys., 57, 335

Zaire, B., Donati J.-F., Klein, B. 2022, MNRAS, 513, 2893